References

[1] K. C. Kao, "Dielectric surface waveguides," presented at the URSI General Assembly, Ottawa, Canada, Paper 6-3.2, Aug. 18–28, 1969.
[2] M. M. Z. Kharadly and J. E. Lewis, "Properties of dielectric-tube waveguides," *Proc. Inst. Elec. Eng.*, vol. 116, pp. 214–224, Feb. 1969.
[3] M. Sugi and T. Nakahara, "O-guide and X-guide: An advanced surface wave transmission concept," *IRE Trans. Microwave Theory Tech.*, vol. MTT-7, pp. 366–369, July 1959.
[4] T. Nakahara and N. Kurauchi, "Millimeter waveguides with applications to railroad communications," in *Advances in Microwaves*, L. Young, Ed. New York: Academic, 1969, vol. 4, p. 191.
[5] K. C. Kao and G. Hockham, "Dielectric-fibre surface waveguides for optical frequencies," *Proc. Inst. Elec. Eng.*, vol. 113, pp. 1151–1158, July 1966.
[6] W. K. McRitchie and J. C. Beal, Dep. Elec. Eng., Queen's Univ., Canada, private communication.
[7] G. L. Yip, "Launching efficiency of the HE_{11} surface wave mode on a dielectric rod," *IEEE Trans. Microwave Theory Tech. (1970 Symposium Issue)*, vol. MTT-18, pp. 1033–1041, Dec. 1970.
[8] M. M. Astrahan, "Guided waves on hollow dielectric tubes," Ph.D. dissertation, Northwestern Univ., Evanston, Ill., 1949.
[9] W. C. Jakes, "Attenuation and radiation characteristics of dielectric tube waveguides," Ph.D. dissertation, Northwestern Univ., Evanston, Ill., 1949.
[10] D. G. Kiely, *Dielectric Aerials*. London: Methuen, 1953.

Systematic Design of Stacked-Crystal Filters by Microwave Network Methods

ARTHUR BALLATO, SENIOR MEMBER, IEEE, HENRY L. BERTONI, MEMBER, IEEE, AND THEODOR TAMIR, SENIOR MEMBER, IEEE

Abstract—**A class of novel frequency-selective devices, called stacked-crystal filters, is discussed in terms of a microwave network approach that leads to a systematic procedure for their analysis and design. These devices consist of two or more crystal plates that are stacked together, with thin electrodes being provided between some or all of the adjacent interfaces for the purpose of translating mechanical properties into electrical signals via piezoelectric coupling. In such a configuration, the electromechanical coupling that occurs at the plate surfaces produces selective interactions between the elastic modes in each crystal plate, as well as between these modes and all of the modes in the other plates included in a stack. A judicious combination of materials and dimensions can therefore provide a very wide range of desired filtering characteristics.**

For stacks with thin plates, only three thickness modes appear in each plate and they can be described in terms of three transmission lines; their coupling at the plate surfaces is then expressible in terms of ideal transformers that represent the mechanical junction between two adjacent plates. The interface electrodes appear as a set of terminals, to which are attached capacitors and another set of ideal transformers that represent the piezoelectric drive. In this manner, each plate can be rigorously described in terms of a well-defined network that serves as a building block. A stack consisting of any number of plates can therefore be regarded as the connection of an appropriate number of such building blocks, thus reducing a complicated mathematical problem to a systematic representation that can readily be handled by conventional techniques. A simple example of a two-layer quartz device operating on these principles is given. The simulated behavior obtained from the exact equivalent network discloses that wide-band filters may be designed. Construction of such devices can be expected to yield robust, miniature filters of high performance possessing a large diversity of desired characteristics.

Manuscript received December 20, 1972; revised June 25, 1973. The work of A. Ballato was supported by USAECOM, Ft. Monmouth, N.J. This paper is based on part of a dissertation submitted by A. Ballato to the Faculty of the Polytechnic Institute of New York, Brooklyn, N.Y., in partial fulfillment of the requirements for the Ph.D. degree in electrophysics in June 1972. The work of H. L. Bertoni and T. Tamir was supported by the Joint Services Electronics Program under Contract F44620-69-C-0047.

A. Ballato is with the U.S. Army Electronics Technology and Devices Laboratory, U.S. Army Electronics Command, Fort Monmouth, N.J. 07703.

H. L. Bertoni and T. Tamir are with the Department of Electrical Engineering and Electrophysics, Polytechnic Institute of New York, Brooklyn, N.Y. 11201 (formerly Polytechnic Institute of Brooklyn).

I. Introduction

PIEZOELECTRIC crystal plates that vibrate mechanically in response to an applied voltage have long been used as compact, rugged, very stable and low-loss one-port resonant elements in frequency-selective circuits. In this paper, a method is given for representing and analyzing a new class of bulk-wave crystal filters, which are formed by stacking two or more crystal plates with electrodes between them [1]. One can thus expect to achieve filters that take advantage of all the desirable properties of crystal plates and to exploit the diversity obtained by joining plates made of different materials. A principal contribution of this study is the development of new equivalent networks, which make possible the systematic investigation of these *stacked-crystal* filters.

The traditional crystal filter consists of an assembly of individual crystal resonators that are wired into an

appropriate network [2]. Coupling among the resonators takes place entirely electrically, this being the source of some of the limitations on these devices. A more recent development is the *monolithic* filter [3], in which two or more pairs of electrodes are placed laterally adjacent to each other on a single crystal plate to permit acoustic coupling between resonators. In general, these filters permit a size reduction over discrete-resonator units, but the operating characteristics are not greatly different, and a restriction to relatively narrow bandwidths at VHF frequencies is a drawback common to both types of crystal filters. Also because the plate thickness must be of the order of wavelength, the lateral size required for monolithic filters makes them fragile and difficult to fabricate for frequencies in the range of 100 MHz and higher. Since the stacked-crystal filters are built by vertical stacking rather than lateral extension, they do not suffer from this limitation.

The realization of stacked-crystal filters requires the exploitation of multimode coupling which occurs at the interfaces between adjacent plates. For a single resonant element, the analysis is relatively simple and has been carried out [4], [5]. However, as no analysis has been available for the much more complex case of stacked crystals, a principal portion of the present paper is devoted to developing a general approach for the analysis of these devices. This approach is based on a representation of stacked crystals by exact equivalent networks that permit a systematic analysis of the effects due to interface coupling between all of the thickness modes in the plate. In these networks, each of the three plane-wave modes in a single-layer material is represented in the bulk by an acoustic transmission line, which is physically equal in length to the thickness of that layer; in general, the three transmission lines possess unequal characteristics. At the interface between any two layers, the pertinent six transmission lines (three from each side) are interconnected by transformer elements. Incorporation of the piezoelectric drive mechanism requires an additional simple network, which is connected only at the transformer terminals, thus providing further coupling between the transmission lines.

Equivalent-circuit representations have long been used to characterize the behavior of piezoelectric vibrators and transducers [6]–[8]. However, these have invariably been single-mode representations which are inadequate to deal with the multimode situation used in the stacked-crystal filter realization.[1] The networks presented here overcome this difficulty and have the additional advantage of being pictorial as well as schematic; they thus account in a simple, physically satisfying manner, for the spatial propagation of the three plate waves and for their coupling at the plate boundaries, via both the piezoelectric effect and the mechanical boundary conditions.

More recently, a transmission-line representation for the propagation of guided acoustic waves, including plane waves, has been developed [9]. In addition, a description of plane-wave scattering at interfaces has been formulated in terms of the coupling of transmission lines through lumped-element networks [10]. While these transmission-line and network representations are limited to the case of isotropic media, the transmission-line representation is general in that it applies to acoustic waveguides of arbitrary cross section, and both transmission lines and networks are applicable to plane waves obliquely incident on an interface. The reflection symmetry of the guide region in the plane normal to the direction of propagation (or parallel to the interface in the case of plane waves), resulting from the restriction to isotropic media, provides a basis for associating each acoustic-field component with either the voltage or current.

The transmission lines and networks discussed here apply to piezoelectric materials, which are therefore anisotropic, but they are restricted to plane waves whose direction of propagation is normal to the interfaces. Because, in general, anisotropic media are not reflection symmetric in planes normal to the direction of propagation, the basis for associating acoustic-field components with voltage or current differs somewhat from that used for isotropic media [9], [10]. As a result, the transmission-line and network representations for the two cases differ in certain details, although both are entirely self-consistent and exact within the context for which they have been developed. The representation given here is also consistent with previously developed networks for piezoelectric resonators and transducers.

A key feature of the network representation developed here is that the equivalent circuit for a stacked structure is built up by the simple interconnection of basic blocks of identical form, with each block accounting for the behavior of one plate. When an actual structure is to be analyzed, it is therefore no longer necessary to perform an *ab initio* mathematical analysis. Instead, the complete characterizing circuit can be put down by inspection, thus reducing the problem to one of network theory. Similarly, the synthesis of a structure that realizes given performance specifications reduces, via the circuit analog, to a problem in the domain of networks. Since, for practical applications, the stacked-crystal device is part of a larger, completely electrical circuit, the electrical representation of the mechanical portion provides a uniformity that lends itself to optimization of the overall electromechanical system. Because the equivalent networks are a pictorial description of the mode interactions, they can greatly aid the designer in selecting interactions that produce a desired filter response. The network description also gives immediate access to computer-aided circuit-design programs, which greatly facilitates the analysis.

In the following sections, the equations governing

[1] A paper by Onoe, *Trans. Inst. Elec. Eng.* (Japan), vol. 55A, pp. 239–244, May 1972, in Japanese, was brought to our attention by a reviewer. This paper has a multimode representation for the plate but contains lumped elements with transcendental functional variation.

acoustic-wave propagation in unbounded piezoelectric crystals are cast into transmission-line form, after which the network realization for the plate is derived, and the normal-coordinate impedance matrix is given. The problem of stacking plates requires a boundary network to account for the mechanical coupling between the transmission-line networks representing each plate. The general coupling network is derived and applied to the practical case of welded contact between plates. The paper concludes with an illustrative example in which a computer simulation is used to generate the filter-response function for a simple two-layer structure composed of quartz plates of varying relative orientation. This example demonstrates the application of these networks and concepts to the development of actual devices, and illustrates the systematic, efficient, and practical aspects of the network characterization developed in the present work.

II. Equivalent Network for a Single Plate in Normal Coordinates

We shall first obtain a representation for the bulk waves within a plate and, at the same time, account for the piezoelectric effect within this region. However, the mechanical restrictions imposed by the boundary conditions will have to be separately accounted for as an additional effect; this will be discussed in Section III.

A. Acoustic Plane Waves in Unbounded Piezoelectric Media

To establish notation, and also to introduce transmission-line concepts in the present context, we shall briefly consider the pertinent equations for the description of plane acoustic waves in a homogeneous, linear, but arbitrarily anisotropic, piezoelectric substance. The three modes, which are allowed for any assumed propagation direction, have motions that are coupled by the elastic and piezoelectric constants; a normal coordinate transformation uncouples them, and is shown to provide a set of first-order differential equations which are to be compared with the Heaviside equations for a transmission line.

Notation and definitions regarding crystal axial conventions, orientation, and constitutive relations agree, for the most part, with the 1949 *Standards on Piezoelectric Crystals* [11]. In agreement with usual tensor notation [4], a subscripted index preceded by a comma indicates differentiation with respect to the space coordinate having that subscript, and the summation convention for repeated indices is employed.

We use, T, u, S, D, and E to represent stress, mechanical displacement, strain, electric displacement, and electric field, respectively, while ρ and φ are the mass-density and electric potential, respectively. The material parameters c^E, e, and ϵ^S are the elastic stiffnesses at constant electric field, the piezoelectric stress constants, and dielectric permittivities at constant strain, respectively. A segment of the plate is indicated in Fig. 1, where x_3 is the coordinate normal to the plate surfaces.

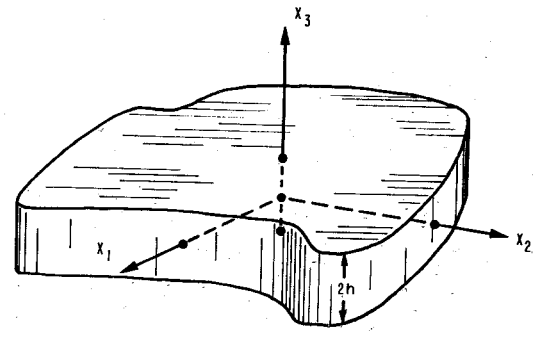

Fig. 1. Segment of a laterally unbounded crystal plate of thickness $2h$, with laboratory coordinates x_i superimposed. For the thickness modes considered, all fields vary only along the thickness coordinate x_3.

The pertinent sets of equations which have to be solved simultaneously are (see [4]): the stress equations of motion, corresponding to Newton's equations; the equations defining mechanical strain; the divergence relation from Maxwell's equations, in the absence of free charge; the electric field-electric potential relations, in the quasi-static approximation; and the linear piezoelectric constitutive relations characterizing the medium [11]. Assuming field variations only along the direction of propagation, x_3, and a time factor $\exp(+j\omega t)$, henceforth omitted, these equations take the form

$$T_{3j,3} = -\rho\omega^2 u_j \tag{1}$$

$$D_{3,3} = 0 \tag{2}$$

$$T_{3j} = c_{3jk3}{}^E u_{k,3} + e_{33j}\varphi_{,3} \tag{3}$$

$$D_3 = e_{3k3}u_{k,3} - \epsilon_{33}{}^S\varphi_{,3}. \tag{4}$$

Here and elsewhere, a Latin index has the range 1,2,3. Only the three stress components T_{3j} are considered here since only they govern the plate motion and take part in the boundary conditions at the plate surfaces.

Substituting (4) into (2) gives

$$\varphi_{,33} = (e_{3k3}/\epsilon_{33}{}^S)u_{k,33}. \tag{5}$$

We treat the case of an exciting electric field in the thickness direction which is produced by electrodes on the plate surfaces, and is referred to as *thickness excitation of thickness modes* (TETM). As a result, φ varies only with x_3, and integration of (5) yields

$$\varphi = (e_{3k3}/\epsilon_{33}{}^S)u_k + a_3x_3 + b_3; \tag{6}$$

the integration constants a_3 and b_3 are determined by the electrical boundary conditions imposed. Insertion of (6) into (4) shows D_3 to be a spatial constant given by

$$D_3 = -\epsilon_{33}{}^S a_3 \tag{7}$$

so that the longitudinal component of the electric displacement is independent of x_3.

The three stress components T_{3j} (x_3) in (1) and (3) represent the force–density vector acting across a plane normal to x_3. We will designate this vector by $t_j(x_3)$. Moreover, when (6) is substituted into (3) it is found that T_{3j} can be separated into two parts as

$$T_{3j} \equiv t_j = \bar{t}_j + \tilde{t}_j \tag{8}$$

where

$$\bar{t}_j = e_{33j}a_3 \tag{9}$$

and

$$\tilde{t}_j = \bar{c}_{3jk3}u_{k,3}. \tag{10}$$

Here

$$\bar{c}_{3jk3} = c_{3jk3}{}^E + e_{33j}e_{3k3}/\epsilon_{33}{}^S \tag{11}$$

are the "piezoelectrically stiffened" elastic stiffnesses at constant normal electric displacement and constant tangential electric field. The vector $\tilde{t}_j$ is solely a consequence of the particle motion, whereas $\bar{t}_j$ is directly produced by the electric field $-a_3$ in the x_3 direction.

Equation (10) is one of the equations of motion of the particles, and when substituted into the other equation of motion, (1), gives

$$\bar{c}_{3jk3}u_{k,33} + \rho\omega^2 u_j = 0 \tag{12}$$

which shows that the components u_k are coupled through the elastic constants.

Equation set (12) may be solved by assuming the displacement vector u_k (x_3) to be of the form $\beta_k \exp(\pm j\kappa x_3)$, which will satisfy (12) provided

$$(\bar{c}_{3jk3} - c\delta_{jk})\beta_k = 0 \tag{13}$$

with

$$c = \rho\omega^2/\kappa^2. \tag{14}$$

To obtain a nontrivial solution to (13), the determinant of the matrix multiplying β_k must vanish. The determinant yields a cubic in c, which has three real, positive roots $c^{(m)}$, from which three real wavenumbers κ_m may be obtained from (14) for a specified value of ω. Each $c^{(m)}$ also determines a set of ratios among the components β_{km} of the corresponding eigenvector. These components may be taken to be real, and when the eigenvectors are normalized to unity, the resulting β_{km} are then the direction cosines of the particle displacement for each of the three plane-wave modes $(m = 1,2,3)$. The three vectors β_{k1}, β_{k2}, and β_{k3} are orthogonal, and are the normal coordinates of the material. Using these as a basis [12], [5], we define transformed force–density, displacement, and piezoelectric coefficient components by

$$t_m{}^0 = \beta_{km}t_i \tag{15a}$$

$$u_m{}^0 = \beta_{km}u_i \tag{15b}$$

$$e_m{}^0 = \beta_{km}e_{33i}. \tag{15c}$$

Because the eigenvectors are orthonormal, the inverse transformations have as coefficients β_{mk}.

B. Network Representation of a Plate

When the separation expressed by (8) is made in the transformed system, it is found that, for each mode m, the particle displacement $u_m{}^0$ and the vector $\tilde{t}_m{}^0$ are parallel. We may therefore write

$$\tilde{t}_m{}^0 = \frac{1}{A}V_m(x_3) \tag{16a}$$

$$v_m{}^0 = j\omega u_m{}^0 = -I_m(x_3). \tag{16b}$$

Here $V_m(x_3)$ and $I_m(x_3)$ describe the x_3 dependence of the modal stress vector and particle velocity, respectively, and A is a suitable area normal to the direction of propagation.

Substituting (16) into (1) and (10), it is found with the help of (8), (13), and (15) that V_m and I_m satisfy

$$V_{m,3} = -j\kappa_m Z_m I_m \tag{17a}$$

$$I_{m,3} = -j\kappa_m \frac{1}{Z_m}V_m \tag{17b}$$

where

$$Z_m = A(\rho c^{(m)})^{1/2}.$$

Equations (17) are the Heaviside transmission-line equations [13]. Thus V_m and I_m may be thought of as the voltage and current on a modal transmission line having characteristic impedance Z_m and wavenumber κ_m. With this viewpoint, each plane-wave mode may be modeled by a transmission line as in Fig. 2, with the understanding that the actual stress vector $\tilde{t}_m{}^0$ and particle velocity $v_m{}^0$ are to be recovered via (16). The positive senses of V_m and I_m along the transmission lines are indicated in Fig. 2.

We consider now the modeling of the potential (6) and the stress vector $\bar{t}_j$ of (9) by the equivalent circuit. In order to show that the presence of these field quantities is correctly accounted for by the equivalent circuit of Fig. 2, we first derive expressions for the potential difference between the surfaces of the plate and the components of $\bar{t}_j$ along the eigenvectors β_{km}.

The electrical potential between the surfaces of the plate is given by the difference between $\varphi(+h)$ and $\varphi(-h)$, where φ is given in (6). For convenience, we define the capacitance C_0 and the dimensionless numbers n_m via the relations

$$C_0 = A\epsilon_{33}{}^S/(2h) \tag{18}$$

$$n_m = Ae_m{}^0/(2h). \tag{19}$$

Recognizing that the particle displacement u_k (x_3) in (6) can be written as a sum of the modal particle displacements $u_m{}^0(x_3)$, and with the help of (16b), (18), and (19),

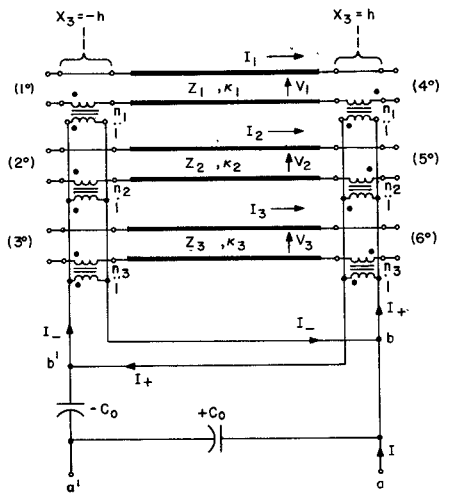

Fig. 2. Seven-port normal-mode equivalent circuit for the crystal plate of Fig. 1, but without mechanical boundary networks and loads.

it is found that

$$[\varphi(+h) - \varphi(-h)] = 2ha_3 - \sum_m \frac{n_m}{j\omega C_0} \cdot [I_m(+h) - I_m(-h)]. \quad (20)$$

The total force $AT_{3j}(\pm h)$ over the area A at the surfaces of the plate is seen from (8) to be the sum of $A\bar{t}_j$ and the sum of $A\bar{t}_m{}^0(\pm h)$ for the three modes. In order to include the force $A\bar{t}_j$ into the network, we resolve it into its components $\bar{V}_m$ along the three orthogonal vectors β_{km}. Thus from (9), (19), and (15c)

$$\bar{V}_m = A\bar{t}_k\beta_{km} = n_m(2ha_3) \quad (21)$$

where the factor $2ha_3$ has been displayed since it represents the contribution to the potential between the plate surfaces from the uniform field along x_3. Recalling from (16a) that V_m measures the force $A\bar{t}_m{}^0$ along β_{km}, it is seen that $V_m(\pm h) + \bar{V}_m$ gives the total force along β_{km} at the plate surfaces.

Equations (20) and (21) are modeled in the equivalent circuit of Fig. 2 by the ideal transformers at the ends of the transmission lines and the series capacitor of value $-C_0$. The terminals $a - a'$ represent the actual electrical terminals for the electrodes on the surface of the plate. The potential of node a above a' is given by $[\varphi(+h) - \varphi(-h)]$. The voltage $2ha_3$ is the potential of node b above node b'. For ideal transformers, the dot convention is used to indicate which terminal of the secondary has positive (negative) voltage when the voltage at the dot on the primary side is positive (negative). Also, if current flows in (out) at the dot on the primary, it will flow out (in) at the dot on the secondary.

The orientation of the dots on the ideal transformers is such that the voltage $2ha_3$ across the primaries reflects itself so as to add the secondary voltage $n_m(2ha_3)$ to the voltage $V_m(\pm h)$ at either end of each transmission line. Thus from (21) the voltage at the mechanical terminals (1°)–(6°), and hence the component of AT_{3j} along β_{km}, will be $\bar{V}_m + V_m(\pm h)$. In other words, the network properly gives the stress at the surfaces of the plate.

The current on the lower wire of each transmission line in Fig. 2 is in the opposite direction to that on the top wire. Hence in view of the dot convention, the currents I_+ and I_- in Fig. 2 are seen to be

$$I_\pm = \sum_m n_m I_m(\pm h). \quad (22)$$

Since the current through the capacitor $-C_0$ from node a' to b' is $[I_- - I_+]$, the voltage $V_{b'a'}$ of b' above a' is the negative of the voltage drop across $-C_0$, and hence

$$V_{b'a'} = -\frac{1}{j\omega(-C_0)}[I_- - I_+]. \quad (23)$$

Because nodes a and b are at the same potential, the voltage $[\varphi(+h) - \varphi(-h)]$ between nodes a and a' is equal to $V_{b'a'}$ plus the voltage $2ha_3$ of node b above b'. In view of (22), this statement is exactly that given in (20). Thus the network properly models the voltage relationship (20).

To complete the justification of the equivalent circuit, it is necessary to show that the current I in Fig. 2 is the one that actually occurs at the electrodes on the plate surfaces. In view of (7), the total current flowing into the electrodes at $x_3 = +h$ is equal to the displacement current $j\omega A\epsilon_{33}{}^S a_3$. From the network, it is seen that the current I is given by

$$I = j\omega C_0[\varphi(+h) - \varphi(-h)] + I_+ - I_-. \quad (24)$$

With the help of (20) and (22), this current is found to equal the total displacement current.

In summary, the network of Fig. 2 correctly represents the transmission line (17), the piezoelectrically induced stress (21) due to the uniform field, and the displacement current $-j\omega AD_3$. These relations, together with the appropriate definitions and the eigenvalue equation (13) are equivalent to the dynamic equations (1)–(4) that govern the plate motion. The network is therefore an exact representation of the plate motion and its coupling to an applied voltage. Note that in Fig. 2, the voltage and current at the mechanical ports (1°)–(6°) are equal to the components of the force AT_{3i} and the negative particle velocity $-v_i$ along the orthonormal eigenvectors β_{im}. In Section III, it is shown that a network of ideal transformers will convert the components along the eigenvectors to the components along the x_i coordinates of Fig. 1.

C. Impedance Matrix Representation

The motion of the plate, as viewed from its surfaces, may also be described by a seven-port impedance matrix. In Fig. 3(a) we enumerate the seven pairs of port variables that completely describe the electromechanical behavior of the plate in Fig. 1. These ports consist of the six components of force $AT_{3j}(\pm h)$ along the x_i coordinates, three

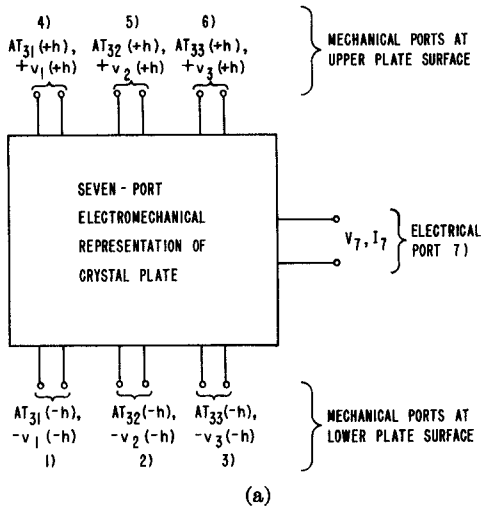

(a)

$$[z^0] = \begin{bmatrix} \frac{Z_1}{j\tan\theta_1} & 0 & 0 & \frac{Z_1}{j\sin\theta_1} & 0 & 0 & \frac{n_1}{j\omega C_0} \\ 0 & \frac{Z_2}{j\tan\theta_2} & 0 & 0 & \frac{Z_2}{j\sin\theta_2} & 0 & \frac{n_2}{j\omega C_0} \\ 0 & 0 & \frac{Z_3}{j\tan\theta_3} & 0 & 0 & \frac{Z_3}{j\sin\theta_3} & \frac{n_3}{j\omega C_0} \\ \frac{Z_1}{j\sin\theta_1} & 0 & 0 & \frac{Z_1}{j\tan\theta_1} & 0 & 0 & \frac{n_1}{j\omega C_0} \\ 0 & \frac{Z_2}{j\sin\theta_2} & 0 & 0 & \frac{Z_2}{j\tan\theta_2} & 0 & \frac{n_2}{j\omega C_0} \\ 0 & 0 & \frac{Z_3}{j\sin\theta_3} & 0 & 0 & \frac{Z_3}{j\tan\theta_3} & \frac{n_3}{j\omega C_0} \\ \frac{n_1}{j\omega C_0} & \frac{n_2}{j\omega C_0} & \frac{n_3}{j\omega C_0} & \frac{n_1}{j\omega C_0} & \frac{n_2}{j\omega C_0} & \frac{n_3}{j\omega C_0} & \frac{1}{j\omega C_0} \end{bmatrix}$$

(b)

Fig. 3. (a) Seven-port electromechanical representation of a crystal plate. Ports 1), 2), and 3) are the mechanical ports at the lower plate surface $x_3 = -h$. Ports 4), 5), and 6) are the mechanical ports at the upper plate surface $x_3 = +h$. Force and particle velocity components are the mechanical port variables; the port variables at the electrical port 7) are electrical voltage and current. (b) Seven-port electromechanical impedance matrix for the piezoelectric crystal plate of Fig. 1, expressed in normal coordinates.

on the top of the plate and three on the bottom, and the corresponding particle velocities v_i. The seventh pair corresponds to the purely electrical voltage and current at the electrodes.

In order to represent the plate completely, the seven-port impedance matrix $[Z]$ for the box in Fig. 3(a) is required. We can find $[Z]$ most simply by first obtaining the impedance matrix $[Z^0]$ that relates the port variables *expressed in normal coordinates*, as in Fig. 2. The overall impedance $[Z]$ *in laboratory coordinates* is then found from $[Z^0]$ by a similarity transformation. We show in Section III that $[Z]$ is realized simply by attaching additional circuitry to each set of mechanical ports of the network of Fig. 2.

For the realization of $[Z^0]$, we define the port voltages to be

$$V_\pi^0 = AT_{3i}(-h)\beta_{im}, \qquad \pi = m = 1,2,3$$
$$V_\pi^0 = AT_{3i}(+h)\beta_{im}, \qquad \pi = m + 3 = 4,5,6 \quad (25)$$

and V_7^0 is the actual electrical voltage across the electrical terminals. Port currents I_ξ^0, taken positive when flowing into the seven-port, are defined as

$$I_\xi^0 = -v_i(-h)\beta_{im}, \qquad \xi = m = 1,2,3$$
$$I_\xi^0 = +v_i(+h)\beta_{im}, \qquad \xi = m + 3 = 4,5,6 \quad (26)$$

and $I_7^0 = I$ is the actual electrical current, equal to $-j\omega AD_3$.

The normal-coordinate impedance matrix elements $[Z^0]$ have been derived from the network of Fig. 2 and are shown in Fig. 3(b), where

$$\theta_m = 2h\kappa_m. \quad (27)$$

The matrix elements of $[Z]$ are of four types, viz., driving-point impedances, which are either electrical or mechanical, and transfer impedances, which connect either two mechanical ports or a mechanical port to the electrical port. Apart from the mode index number, all the driving-point mechanical impedances are of the same form. The transfer mechanical impedances between the two ports of the plate that have the same value of the mode index number are also equal, as are the corresponding electromechanical mutual impedances, so that $Z_{\pi\xi}^0$ is symmetric. Similar considerations apply to a formulation of the seven-port in terms of admittances. The impedance matrix has, however, the simpler form, because a number of matrix elements are equal to zero.

III. Equivalent Network for the Mechanical Interface

A. The Mechanical Boundary Network

The matrix and network so far described refer to the normal-coordinate system, which was introduced for the purpose of uncoupling the motions of the plate so that they could be represented by three modal transmission lines. From the matrix of Fig. 3(b), the overall impedance matrix $[Z]$ for the plate (with mechanical ports referred the the laboratory coordinate system) is obtained as follows. Defining the mechanical port voltages and currents as the force components $AT_{3i}(\pm h)$ and velocity components $\pm v_i(\pm h)$, the port voltages and currents in Fig. 3(a) are related to those in Fig. 2 by

$$V_\lambda = B_{\lambda\pi}V_\pi^0$$
$$I_\mu = B_{\mu\xi}I_\xi^0 \quad (28)$$

where

$$B_{\lambda\mu} = \beta_{ij}(i,j = 1,2,3; \lambda = i,i+3; \mu = j,j+3)$$

$$B_{77} = 1 \tag{29}$$

$$B_{\lambda 7} = B_{7\lambda} = 0 \qquad (\lambda \neq 7).$$

The overall impedance matrix elements $Z_{\lambda\mu}$ are then found to be related to $Z_{\pi\xi}{}^0$ by the similarity transformation

$$Z_{\lambda\mu} = B_{\lambda\pi} Z_{\pi\xi}{}^0 B_{\xi\mu}. \tag{30}$$

The network representation of (30) requires a network at each set of mechanical ports ($x_3 = \pm h$) in Fig. 2, as prescribed by the orthogonal transformation from the normal-mode coordinates to the laboratory coordinates of Fig. 1. A multiwinding, ideal transformer interconnection that realizes this transformation is given by Carlin and Giordano [14] and is shown in Fig. 4. In the figure, the turns ratios β_{im} are the ith components of the mth eigenvector in the laboratory coordinate frame. The figure may be reversed, and the primaries labeled with the normal coordinate variables; this is achieved by interchanging subscripts on the components of β_{im} for the transformer turns ratios.

By attaching two networks of the form given in Fig. 4 to the network of Fig. 2, the combined circuit becomes an exact characterization of the piezoelectric thickness-mode plate subject to arbitrary boundary loadings. The network of Fig. 2 cannot be used directly for this purpose because the variables at each port are composed of a combination of the actual mechanical boundary conditions. For example, a single compressive stress acting along x_3 upon both plate surfaces appears generally as voltage sources impressed at all six mechanical ports. For the practical case of two plates in welded contact, the boundary conditions require that the stress and velocity components of both plates be continuous. This makes inevitable the introduction of a transformation network between the equivalent circuits representing the two plates, since each circuit is based upon the normal coordinates proper to its own crystal plate, rather than upon the more convenient laboratory coordinates x_i.

In particular instances, the orthogonal transformation networks may simplify or disappear entirely. This may come about for two distinct reasons. First, the β_{im} array may be reduced in complexity as a result of the nature of the crystal and/or the chosen direction of propagation. Second, the boundary impedance seen by the plate surface may bring about a simplification. We consider a simplification of the network due to a special set of β_{im} in the illustrative example of the stacked-crystal filter given in Section IV.

The second type of simplification, due to the form of the boundary impedance, may be illustrated by examining the effect of placing a thin, but heavy, electrode film on a plate surface. If the plating is characterized by a lumped

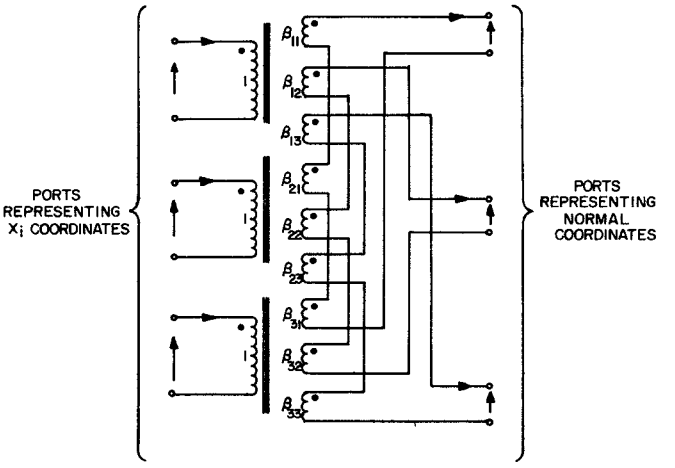

Fig. 4. Ideal transformer realization of an orthogonal transformation: the mechanical boundary network. One of these networks is attached to each side of the network of Fig. 2 to provide the overall network realization of the crystal plate driven in thickness modes. The β_{im} are the direction cosines of the particle motion for the modes (m).

mass m per unit area with its elastic properties neglected, it appears in the equivalent circuit as a set of three inductances, each of value mA, and each attached to one of the x_i-coordinate ports in Fig. 4. At the other ports one then sees the same thing, viz., three inductances of value mA. This comes about because the network of Fig. 4 subjects impedances to similarity transformations, as may be seen from (28)–(30) by allowing the Greek indices to range only over the values 1, 2, and 3. The impedance matrix in question is simply a scalar times the unit matrix so the impedance matrix is therefore unchanged by the transformation. The mechanical transformation network consequently can be omitted, and the inductances placed directly at the normal-coordinate ports of Fig. 2 that represent the surface in question.

B. The Traction-Free Single Plate

As the mass per unit area vanishes, the boundary becomes traction-free, and the inductances are replaced by short circuits. The exact equivalent circuit realizing this situation at both surfaces is shown in Fig. 5. The input admittance, Y_{in} (TETM), seen at port seven, can be readily calculated, and it agrees identically with that given analytically by Yamada and Niizeki [5]. Here the three modal transmission lines are mechanically uncoupled at the boundaries and the piezoelectric effect provides the sole coupling mechanism.

One may use the symmetry of Fig. 5 to simplify the pertinent network. Because of the transformer dot array, the mechanical voltages produced at the ends of each transmission line have the same polarity, and the midpoints of the lines are nodes of mechanical current. We may therefore bisect the network of three transmission lines at their centers, thus obtaining six lines (each of length h), which are open-circuited at the terminals produced by the bisections. The six lines consist of three sets of identical twins, which are all connected in parallel

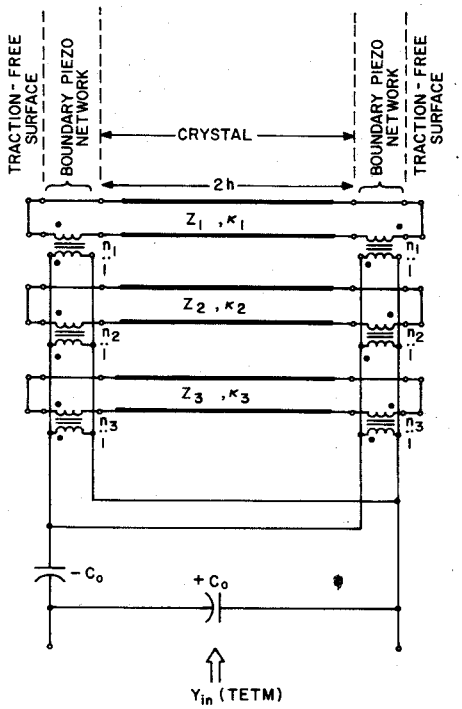

Fig. 5. Equivalent network analog representation of a crystal plate with both surfaces traction-free. The vanishing of the stresses at the boundaries leads to the disappearance of the mechanical boundary networks and to imposition of short circuits at the transmission-line ends.

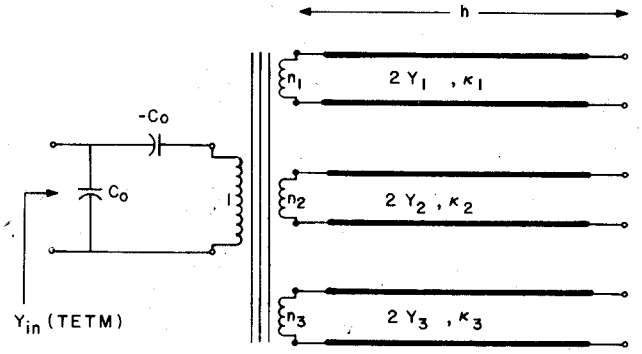

Fig. 6. Bisected version of Fig. 5. The exact equivalent network for a traction-free plate driven by a thickness-directed field is reduced here to its simplest form. The polar nature of the piezo drive leads to excitation of only the antisymmetric modes having vanishing particle displacement at the plate midplane.

through their piezo transformers. Each set of twin lines can be further reduced to a single line, having twice the characteristic admittance of the individual lines. Our manipulations thus lead us to Fig. 6. Here the three modal transmission lines have been connected via a common-core transformer, so that the secondaries are in parallel. Application of standard network techniques has thus brought the circuit realization into a form where the analysis may be made by inspection. Casting the plate problem into network form therefore allows systematic application of highly developed network procedures of analysis and leads to the possibility of an overall optimization of the system performance.

C. Stacking of Two Plates

When two crystal plates are to be brought into welded contact, as shown in Fig. 7, the physical boundary conditions require that the components of traction and displacement be continuous in the laboratory coordinates. The network of Fig. 4 attached to each side of the normal-coordinate network of Fig. 2 produces these stress and displacement components directly at the x_i-coordinate ports. In order to represent the welded contact of two plates, it is only necessary to connect together the x_i-coordinate ports of the mechanical transformation networks that separately represent the two boundaries to be mated, as shown in Fig. 8. This network may be simplified by suppressing the primary loops of the resulting interconnection, thus obtaining the final network for the

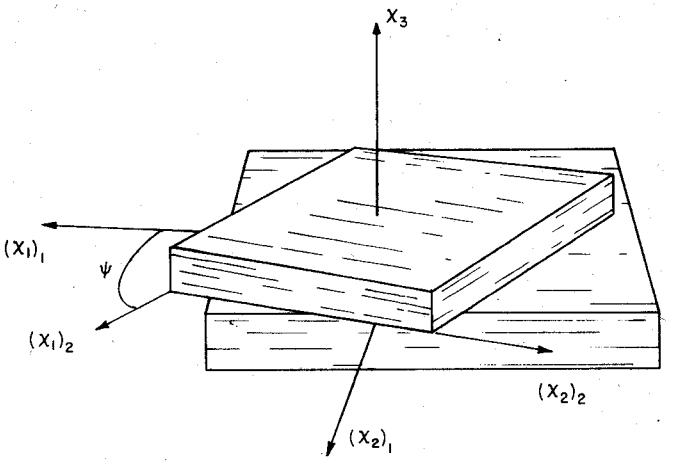

Fig. 7. Two-layer stack of crystal plates showing relative rotation about the common x_3 axis. The illustrative example of Section IV describes the response of a stack of two plates operated as a filter, with input and output sharing the common electrode located at the interface.

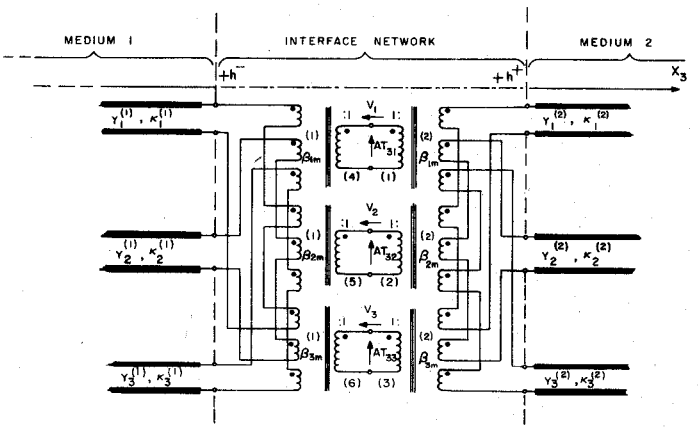

Fig. 8. Exact analog representation of mechanical interface coupling between two crystals having arbitrary anisotropy. Plane-wave propagation is normal to boundary, and piezoelectric drive connections have been omitted for clarity. A thin, massy electrode located at the interface would be represented by insertion of an inductor in series in each of the central loops.

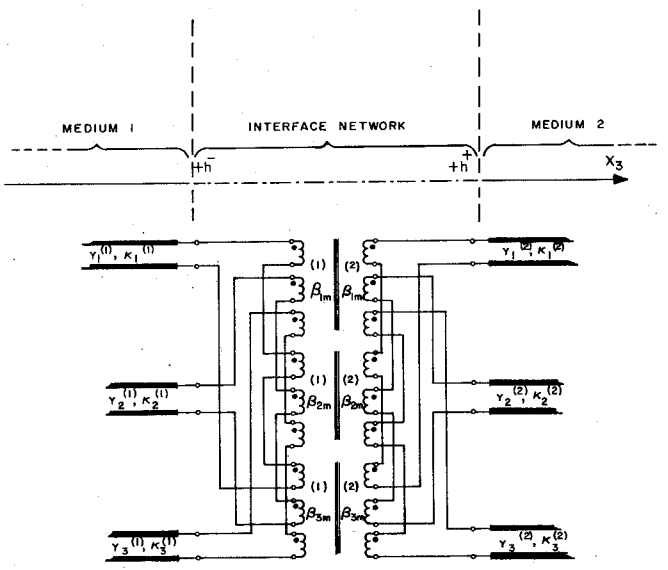

Fig. 9. Mechanical interface network representing welded contact between two crystals in the most general case of anisotropy. This figure is obtained from that in Fig. 8, to which it is equivalent, by suppressing the internal loops in the transformer interconnection.

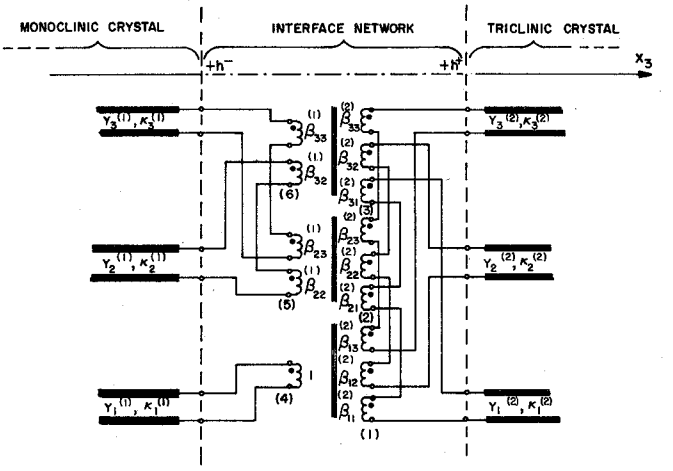

Fig. 10. Exact mechanical interface network specialized to the situation of welded contact between a general triclinic crystal and a crystal of monoclinic symmetry. Piezoelectric interconnections have been omitted for clarity; they may be added in a simple manner, as described in Section III-C.

interface shown in Fig. 9. An additional superscript has been added, where necessary, to distinguish between the two crystals. Fig. 9 is the most general situation involving welded mechanical coupling that may arise between two planar crystal interfaces. All piezoelectric connections have been removed from the figure for clarity. They may readily be grafted on by inserting the piezoelectric drive transformers, in series with each transmission line, in the manner of Fig. 2. The piezoelectric transformer primaries lead off to the electrical port connections of each plate. The practical case of a negligibly thin electrode film shared between the juxtaposed crystal plates at the interface is simply represented by directly connecting the electrical terminals that are adjacent at the boundary. The same applies even if the electrode mass cannot be neglected, except that the inductances that represent the mass are placed in series in each of the primary loops of Fig. 8.

By utilizing the circuit of Fig. 2, augmented by boundary networks to represent each crystal plate, and with the interconnections described to represent satisfaction of welded-interface boundary conditions, the generalization to a stack of any number of plates follows immediately. In a multilayer stack, the electrodes of the individual plates may be connected electrically in series, in parallel, or arbitrarily grouped in a series-parallel combination, as in the case with conventional stacks [15].

A particularization of Fig. 9 that we will use in our illustrative example in the next section is given in Fig. 10. Here we show a welded contact between a general triclinic substance on the right, and a material having monoclinic symmetry on the left. Representing the triclinic crystal is a mechanical interface network in its most general form, as given in either half of the network of Fig. 9. The left-hand side of the interface network of Fig. 10 may be identified, for example, with a rotated Y-cut quartz plate [11]. The rotation destroys the class 32 symmetry, and makes the plate appear, with respect to coordinate axes rotated around the original twofold axis, as a crystal in class 2. We take our x_1 along the twofold crystallographic axis and x_3 along the plate thickness. Then mode (1) is a pure-shear mode, which is the only mode that is piezoelectrically driven in TETM.

If the triclinic crystal is arbitrary, we have to attach piezoelectric transformers to all transmission lines on the right side of the figure. On the other hand, a rotated Y-cut quartz crystal which has been further rotated about the x_3 (thickness) axis with respect to the laboratory frame, appears to be triclinic elastically, but only mode (1) may be driven piezoelectrically in TETM.

The network of Fig. 10 thus represents the situation where two rotated Y-cut quartz plates have been joined, with the laboratory frame coinciding with the x_i set of the left crystal, and the x_1 axis of the right crystal at an angle to the x_1 axis of the other.

IV. Two-Layer Stacked-Crystal Filters

A two-layer stack of crystal plates, with an electrode at the interface in addition to those at the free surfaces, can be used as a filter element by utilizing the two electrical ports as input and output, and arranging the plate thicknesses and orientation angles properly. We consider the plates shown as in Fig. 7 to be in welded contact and to be driven in TETM.

Each rotated Y-cut quartz crystal has the rotational symbol $(YXl)\theta$, the angle θ describing the rotation about the crystallographic X axis [11]. The values of θ, as well as the rotation angle ψ (about the thickness) of one crystal with respect to the other may be independently chosen. Therefore three angles are disposable for a two-layer stack of singly rotated crystals. The relative rotation of the plates about the common x_3 axis provides a means of

investigating the effects of change in the mechanical-interface transformer turns ratios.

In view of the three electrodes, the input and output can be taken in a number of ways; we shall consider the central electrode as common to both input and output. Thus, for instance, the electrode placed on the top plate could lead to the generator, the electrode at the lower plate surface could be connected to the detector, and the central electrode could serve as a common ground. From the results of previous sections it is apparent that even a simple two-layer stack generally possesses six transmission lines which are all coupled together mechanically and also piezoelectrically. For the purposes of the example, we introduce a number of simplifications so that the essential behavior of this class of devices may be demonstrated without an extended discussion.

Because of the completeness with which its material constants are known, and because it preserves so many connections with currently used devices, we choose quartz for the two media in Fig. 7. Specifically, both plates individually are chosen to have the same *crystal-cut* orientation, that of the AT-cut: $(YXl)\theta$, $\theta = +35°15'$. This choice has four major consequences. First, the behavior of single plates of this cut is universally known, so that our filters can be contrasted with known results for quartz filters of standard construction. Second, the selection of the same cut makes the eigenvalues of both plates equal, so that the critical frequencies of each plate (taken separately) are in the same ratios. Third, the lower shear mode is a pure mode, so that the interface network is simplified. Finally, only the pure shear mode in each plate is TETM-drivable, thus simplifying the piezoelectric interconnections.

The overall circuit for this filter is shown in Fig. 11, where the mechanical interface network is that of Fig. 10. The outer surfaces of the plates are traction-free, so that the transmission lines are terminated in short circuits.

Since both plates have the same orientation angle θ, the corresponding transmission lines on each side of the figure are identical. When the *relative* rotation angle ψ is zero, the device becomes identical with a single plate of quartz, except that a central electrode is present. The mechanical network then degenerates into a set of three direct feedthroughs. When $\psi \neq 0°$, the network of Fig. 10 is appropriate and the modal matrix components $\beta_{ij}^{(2)}$, governing the transformer ratios on the right-hand side, are then functions of ψ if the x_j axes of the crystal on the left-hand side are chosen as the reference set.

In a specific numerical illustration, we take the plates to be of equal thickness, which is such that $\omega_1/2\pi = 100$ MHz, where ω_1 is the angular frequency at which the reference plate (taken alone) has its first admittance null. The effect of making the plates of equal thickness is to force the frequencies of both plates to be the same, so that only three rather than six modes have to be considered. Having the overall impedance matrices for each layer, as given in Section II, it is not difficult to obtain the two-port impedance matrix between the electrical ports of the two-layer stack. The top and bottom faces

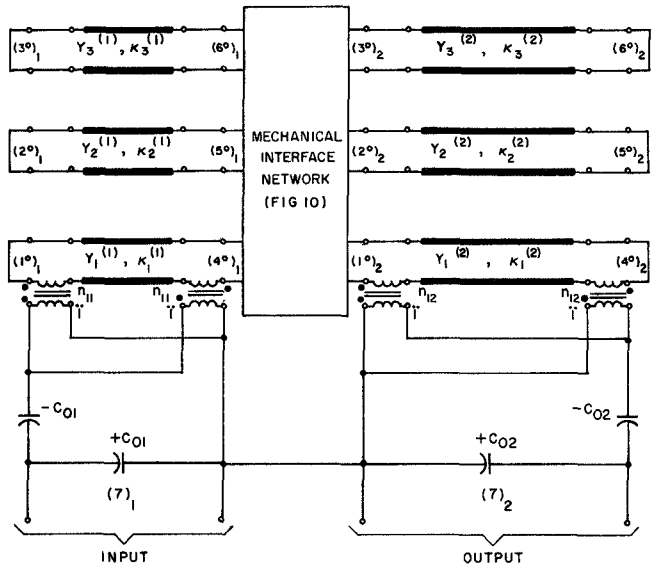

Fig. 11. Complete network representation of the electrical two-port formed by a two-layer stack of crystal plates in welded contact. The outer plate surfaces are free of tractions, and one mode only is taken to be piezoelectrically driven in each crystal. In the general case the interface contact would be represented by the network of Fig. 9; that of Fig. 10 is used for the illustrative example of Section IV.

of the plates are traction-free, so that the transmission lines representing the plates are shorted there; the three internal mechanical ports of each plate are connected together, thus leaving only the electrical ports unconnected. Matrix methods pertinent to the interconnection of networks may be found in [16].[2]

Once the interconnected networks have been characterized by a two-port impedance matrix Z_{ij}, the attenuation may be determined provided the source and load impedances are known. We assume for simplicity that these are equal and purely real, namely

$$Z_{\text{source}} = Z_{\text{load}} = R = 1/(\omega_1 C_0) = 50\ \Omega$$

where the capacitance C_0 refers to the shunt capacitance of a single plate. Then using the equations found, e.g., in Zverev [2], the attenuation loss in decibels, is

$$L(\text{dB}) = 10 \log_{10} \{[Z_{11} + Z_{22}]^2 + [(\det Z)/R + R]^2\} - 20 \log_{10} | 2Z_{12} |.$$

Using all of the preceding simplifying assumptions, we are left with results that are easily described and analyzed. The computer-generated output is plotted in Fig. 12, where the normalized frequency $\Omega = \omega/\omega_1$ is used as the abscissa. Curves are presented for the three angles $\psi = 0°$, 4°, and 8°. When $\psi = 0°$, the stack appears as an asymmetrically driven single plate of thickness $4h$ and, because of the lack of symmetry, the stack possesses resonances at both odd and even integer values of Ω. The only driven

[2] See [14].

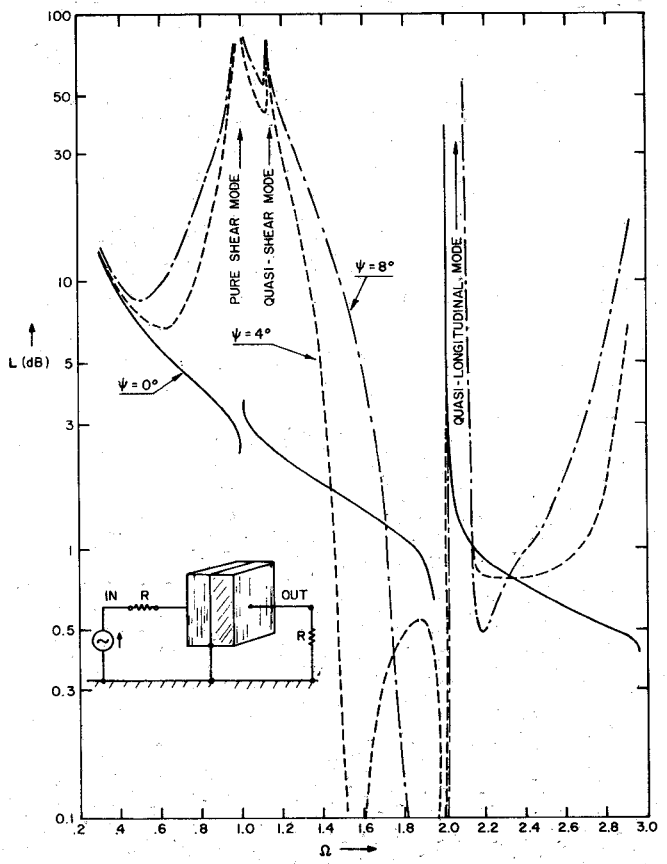

Fig. 12. Attenuation versus frequency for a two-layer stacked-crystal filter comprising 100-MHz AT-cut quartz plates in a 50-Ω system. Frequency is normalized to the lower shear mode. The angle ψ measures the relative rotation of the plates about a common thickness axis. Poles of attenuation occur whenever one of the short-circuited transmission-line ends from Fig. 11 is reflected to the interface to produce an uncoupling. Note the log–log ordinate scale.

mode is the lower shear mode, which is a purely transverse mode. Hence this mode is completely uncoupled from the others, so that any resonances due to them do not appear in the attenuation function. In both cases where $\psi \neq 0°$, the attenuation function has poles at $\Omega = 1.000$, 1.142, and 2.105, corresponding to modal velocities $v^{(i)}$, of 3.328, 3.800, and 7.007×10^3 m/s. An easy way to explain the presence of the poles of attenuation is to recognize that whenever a transmission line becomes one half-wavelength long, the short circuit at the traction-free boundary appears also across the other end of the line and thus uncouples the two plates.

Although the poles are fixed, the shape of the curves may be changed by varying ψ, so that one has a simple means of obtaining different filter responses. Our illustration thus indicates how devices based on these principles might operate and provides an example that is still quite simple and readily interpreted. Even so, the resulting curves for $\psi = 4°$ and 8° already indicate reasonable wide-band filter responses in the region just below $\Omega = 2$; no attempt has been made to optimize these responses in any way. Removing the restriction of equal plate thicknesses will also permit narrow-band filters to be designed as stacked-crystal filters.

The possible filter responses available for even the simplest two-layer structure are very large. Even if the plates are restricted to a single material, each plate cut is specified by two angles in the general case, so with the mutual rotation angle between the plates there are five disposable parameters to which must also be added the ratio of the plate thicknesses. A large area for investigation is available here. Extensions to structures composed of more than two plates, and the use of different materials for each of the plates further widen the possibilities of these devices for frequency selection and control, and signal processing.

V. Conclusion

In this paper, rigorous network analogs have been obtained for configurations of stacked plates excited piezoelectrically. The realization and optimization of practical devices based upon these ideas, however, can best proceed by introducing a step which is intermediate between a circuit and the physical device it represents. This step consists in utilizing the network to simulate the ideal behavior of the device by using computer-aided circuit-design programs. In this way, changes can be made easily without having to resort to a breadboard model each time the effect of some alteration in structure or in composition needs to be known. Since the networks are exact representations of the physical model, they will faithfully reflect the behavior of the devices.

An illustrative example is given that consists of computer-simulated attenuation response curves of a new type of two-layer, integrated, wide-band filter. In this configuration, the frequency-selective device is composed of two media wherein the three modes in each layer are permitted to interact with each other via the mechanical boundary conditions. Mutual shielding or packaging is not required. The device is inherently robust because of its integral construction, and also lends itself readily to miniaturization. By utilizing two or more layers, integral, stacked-crystal filters of this type could readily be made, these being completely compatible with integrated-circuit technology.

References

[1] A. Ballato, H. L. Bertoni, and T. Tamir, "Transmission-line analogs for stacked crystals with piezoelectric excitation," presented at the 83rd Meeting of the Acoustical Society of America, Buffalo, N.Y., Apr. 1972; *J. Acoust. Soc. Amer.* (Abstract), vol. 52, p. 178, paper NN3, July 1972.

[2] a) A. I. Zverev, *Handbook of Filter Synthesis.* New York: Wiley, 1967. b) W. P. Mason, "Use of piezoelectric crystals and mechanical resonators in filters and oscillators," in *Physical Acoustics: Principles and Methods,* vol. I, W. P. Mason, Ed. New York: Academic, 1964, pt. A, ch. 5, pp. 335–416.

[3] a) N. H. C. Reilly and M. Redwood, "Wave-propagation analysis of the monolithic-crystal filter," *Proc. Inst. Elec. Eng.* (London), vol. 116, pp. 653–660, May 1969. b) W. P. Mason, "Equivalent electromechanical representation of trapped energy transducers," *Proc. IEEE,* vol. 57, pp. 1723–1734, Oct. 1969.

[4] H. F. Tiersten, "Thickness vibrations of piezoelectric plates," *J. Acoust. Soc. Amer.,* vol. 35, pp. 53–58, Jan. 1963.

[5] T. Yamada and N. Niizeki, "Admittance of piezoelectric plates vibrating under the perpendicular field excitation," *Proc. IEEE,* vol. 58, pp. 941–942, June 1970.

[6] W. P. Mason, "A dynamic measurement of the elastic, electric

and piezoelectric constants of Rochelle salt," *Phys. Rev.*, vol. 55, pp. 775–789, Apr. 1939.
[7] T. M. Reeder and D. K. Winslow, "Characteristics of microwave acoustic transducers for volume wave excitation," *IEEE Trans. Microwave Theory Tech.*, vol. MTT-17, pp. 927–941, Nov. 1969.
[8] R. Krimholtz, D. A. Leedom, and G. L. Matthaei, "New equivalent circuits for elementary piezoelectric transducers," *Electron. Lett.*, vol. 6, pp. 398–399, June 1970.
[9] A. A. Oliner, H. L. Bertoni, and R. C. M. Li, "A microwave network formalism for acoustic waves in isotropic media," *Proc. IEEE*, vol. 60, pp. 1503–1512, Dec. 1972.
[10] A. A. Oliner, R. C. M. Li, and H. L. Bertoni, "Catalog of equivalent networks for planar interfaces," *Proc. IEEE*, vol. 60, pp. 1513–1518, Dec. 1972.
[11] "Standards on Piezoelectric Crystals, 1949," *Proc. IRE*, vol. 37, pp. 1378–1395, Dec. 1949 (IEEE Standard No. 176).
[12] a) S. A. Basri, "A method for the dynamic determination of the elastic, dielectric, and piezoelectric constants of quartz," *National Bureau of Standards Monograph 9*, U.S. Dep. Commerce, June 1960, 22 pp. b) N. F. Foster, G. A. Coquin, G. A. Rozgonyi, and F. A. Vannatta, "Cadmium sulphide and zinc oxide thin-film transducers," *IEEE Trans. Sonics Ultrason.*, vol. SU-15, pp. 28–41, Jan. 1968.
[13] a) L. B. Felsen and N. Marcuvitz, "Modal analysis and synthesis of electromagnetic fields," Contract AF-19(604)-890, Rep. R-446-55 (a) and (b), Polytechnic Inst. Brooklyn, N.Y., Feb. 1956, 40 pp. (AD93662). b) W. L. Weeks, *Electromagnetic Theory for Engineering Applications*. New York: Wiley, 1964.
[14] H. J. Carlin and A. B. Giordano, *Network Theory: An Introduction to Reciprocal and Nonreciprocal Circuits*. Englewood Cliffs, N.J.: Prentice-Hall, 1964, sec. 3.16, pp. 190–207.
[15] E. K. Sittig, "Transmission parameters of thickness-driven piezoelectric transducers arranged in multilayer configurations," *IEEE Trans. Sonics Ultrason.*, vol. SU-14, pp. 167–174, Oct. 1967.
[16] E. A. Guillemin, *Introductory Circuit Theory*. New York: Wiley, 1953.

Design of Unapodized Surface-Wave Transducers with Spectral Weighting

GRAHAM R. NUDD, SENIOR MEMBER, IEEE, MICHAEL WALDNER, MEMBER, IEEE, AND R. L. ZIMMERMAN, MEMBER, IEEE

***Abstract*—The technique commonly employed to provide a wideband surface-wave transducer with a specific conversion loss as a function of frequency uses the linear frequency-modulation (LFM) (quadratic-phase) design. This provides the necessary dispersion, and apodization is then employed to obtain the required conversion loss. In some applications the apodization presents complications in that the beam generated has nonuniform width, and diffraction and phase-front problems can result. An alternate technique is described that relies on varying the number of effective transducer elements as a function of frequency to provide the conversion-loss variation. As examples of this technique, a flat bandpass filter for a nonlinear convolver and a very large fractional-bandwidth transducer (with spectral weighting to provide sidelobe control) for a memory application are described.**

I. Introduction

In many applications of surface-wave acoustics for signal processing it is necessary to control the insertion loss as a function of frequency across the band of the filter [1]. The conventional technique for achieving this is to build an array with a linear frequency-modulated (LFM) characteristic providing the wide bandwidth and then to apodize the elements within the array to provide the spectral weighting [2]. The apodization can cause problems because of the nonuniform beamwidth it produces and the variation in diffraction losses across the band.

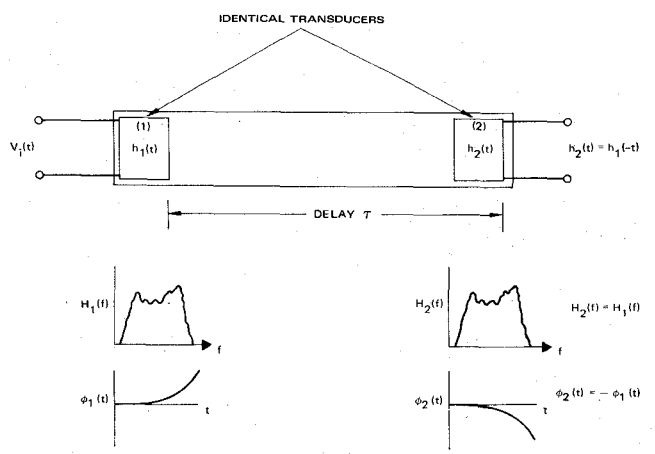

Fig. 1. Schematic of surface-wave filter.

An alternate technique which has found application in a variety of devices and avoids apodization and its associated problems, but provides a controlled insertion loss as a function of frequency, is described here. The technique relies on varying the number of elements within the array that are synchronous at any given frequency. By varying the number of effective elements $N(f)$ as a function of frequency f across the band, the insertion loss can be controlled to provide the desired spectral characteristics. This technique requires control of the finger positions to

Manuscript received January 10, 1973; revised June 17, 1973. This work was supported in part by the Wright-Patterson Air Force Base Avionics Laboratory under Contract F33615-72-C-1070, and in part by the Rome Air Development Center under Contract F30602-71-C-0196.

The authors are with Hughes Research Laboratories, Malibu, Calif. 90265.